Supporting Information

Silva et al. 10.1073/pnas.1016616108

SI Materials and Methods

Materials. Monomeric (G-) actin and myosin II were purified from rabbit psoas skeletal muscle without column purification (1, 2). G-actin was stored at −80 °C in G-buffer (2 mM Tris-HCl, 0.2 mM Na_2ATP, 0.2 mM $CaCl_2$, 0.2 mM dithiothreitol (DTT), 0.5 mM NaN_3, pH 8.0). Myosin II was stored at −20 °C in a high-salt buffer with glycerol (0.6 M KCl, 25 mM KH_2PO_4, 10 mM EDTA, 1 mM DTT, pH 6.5, 50% w/w glycerol). Fresh myosin solutions were prepared daily by dialysis against AB300 buffer (300 mM KCl, 4 mM $MgCl_2$, 1 mM DTT, 25 mM imidazole, pH 7.4). Protein concentrations were determined by absorption measurements at 280 nm for myosin and 290 nm for G-actin, using extinction coefficients of 0.53 cm^2/mg for myosin and 1.1 cm^2/mg for G-actin, respectively (1). G-actin labeled with biotin was purchased from Cytoskeleton (Tebu Bio), and G-actin labeled with Alexa488 or Alexa568 was purchased from Invitrogen. Streptavidin was obtained from Pierce (Thermo Fischer), and creatine phosphate (CP) and creatine kinase (CK) were obtained from Roche Diagnostics. Other chemicals were purchased from Sigma Aldrich. ATP was prepared as a 100 mM MgATP stock solution using equimolar amounts of Na_2ATP and $MgCl_2$ in a 10 mM imidazole-HCl buffer (pH 7.4).

Fluorescent Labeling of Myosin II Motor Proteins. Myosin II was labeled with DyLight NHS Ester 488 or 594 (Perbio) according to a protocol adapted from refs. 3 and 4. This labeling preserves the reversible assembly of myosin into synthetic filaments and its actin-activated MgATPase activity. All procedures were performed at 4 °C. Myosin was first assembled into synthetic filaments by a 2 h dialysis against a low-salt buffer (10 mM Hepes, 50 mM KCl, 0.2 mM EGTA, 2 mM MgATP, 2 mM $MgCl_2$, pH 7.0). To the clear top layer of the dialyzed myosin, a 20-fold molar excess of the fluorescent dye (from a 40 mM stock in dimethylsulfoxide) was slowly added. After incubation on ice and in the dark for 1 h, the labeling reaction was stopped by addition of 20 mM D-Lysine. Unreacted dye was removed by dialyzing the myosin solution for at least 3 h against a buffer containing 10 mM Hepes, 50 mM KCl, and 0.2 mM EGTA at pH 7.0. After addition of 10 mM $MgCl_2$, the fluorescent myosin filaments were precipitated by centrifugation for 10 min at 8,000 g. The pellets were resuspended in a minimal volume of high-salt buffer favoring filament disassembly (600 mM KCl, 50 mM KH_2PO_4, 1 mM DTT, pH 7.5) and the solution was dialyzed against the same buffer overnight. Aggregates were removed by centrifugation (10 min at 8000 g). We obtained labeling stoichiometries between 1.7 and 2.7 dye molecules per myosin molecule, based on the ratio between the absorbance at 280 nm and the absorbance of the dye at its maximum. The labeled myosin was stored at −20 °C in monomeric form in a high-salt buffer with glycerol (600 mM KCl, 50 mM KH_2PO_4, 1 mM DTT, pH 7.5 with 50% glycerol).

Actomyosin Network Reconstitution. Reconstituted networks were prepared in assembly buffer with final concentrations of 25 mM imidazole-HCl, 50 mM KCl, 0.1 mM MgATP, 2 mM $MgCl_2$, 1 mM DTT, and pH 7.4. To prevent ATP depletion, we included a regeneration mixture containing 11.76 mM creatine phosphate, 766 units/mL creatine kinase (5). To prevent photobleaching, we added 2 mM Trolox. The actin concentration was fixed at 23.8 μM (1.0 mg/mL). The average length of the actin filaments measured by fluorescence microscopy and analysis of 3,711 filaments was 6 μm (analyzed using the NeuronJ plugin of ImageJ). The actin network was labeled by mixing fluorescent G-actin and unlabeled actin in a 1:20 molar ratio. We inserted a controlled number of cross-link points into the actin filaments by copolymerizing biotinylated G-actin with unlabeled G-actin in a molar ratio varying from zero to 1:20. The number of available cross-link points per actin filament is about 14 at the highest biotin density, assuming that cross-link points occur in equally probable random placement along the filaments. Excess streptavidin (streptavidin:actin molar ratio of 1:25) was included to form cross-links between the biotinylated actin filaments. The molar ratio between myosin and actin was varied between 1:300 and 1:50. For all samples myosin was mixed with all buffers first, allowing the formation of synthetic filaments at room temperature. Finally, G-actin was added and the sample was quickly transferred to a flow cell composed of a glass slide and coverslip separated by a 25 μm FEP spacer (fluorinated ethylene propylene copolymer, Goodfellow) and closed with silicone grease (Baysilone, GE Bayer). The final structure of the patterns was unaffected when myosin monomers were added last to the polymerizing actin. However, this mixing sequence slowed the process of active coalescence down. Actin polymerization did not seem to affect the self-organization process: a fully formed actin network was present before any spatial inhomogeneities in actin or myosin density appeared. Rheology experiments suggested that network formation was complete within about 30 min (Fig. S4*B*). As a further test that actin polymerization has no influence on self-organization, we mixed myosin filaments with preformed actin filaments, and indeed found the same final contracted states (Fig. S6*B*).

Assembly and Characterization of Myosin Synthetic Filaments. The low-salt conditions of the assembly buffer induce the spontaneous assembly of myosin by its tail-region into synthetic filaments (6). Structural studies using electron microscopy (EM) showed that these filaments are structurally homologous to native thick filaments in muscle in terms of bipolarity and subunit periodicity (7). The filaments consist of a central bare zone where the myosin molecules are antiparallel, flanked on both sides by a parallel array of myosin motors with a crown of 3 myosin molecules every 14.3 nm. We determined the length distribution of the myosin filaments by atomic force microscopy (AFM) imaging of myosin filaments assembled for 5 min at room temperature at a concentration of 0.1 μM in the same assembly buffer used for networks. The assembled filaments were pipetted into freshly cleaved mica surfaces coated with nitrocellulose. The samples were imaged by AFM using a Veeco Dimension 3100 atomic force microscope (Veeco) in tapping mode with tips of the type MPP-12100-10 (Veeco). The filament length and diameter were measured using WSxM software (Nanotec). The diameter was obtained as the average of the filament height determined across a profile along the filament contour.

Contractility from Asymmetric Load Response. Perhaps surprisingly, microscopically polar, directed motor activity can give rise to net contractility even in macroscopically apolar structures, provided that the load response is asymmetric. Individual actin filaments are highly asymmetric in their response on the micrometer scale, in that they strongly resist extension, yet buckle easily under compressive loads of less than a piconewton. We approximate this load response as that of an inextensible macroscopic rope with zero resistance to compression. For networks of such actin filaments cross-linked on the micrometer scale, the network load response is also expected to be asymmetric. On this scale, such networks are inhomogeneous with loose or floppy regions that

we refer to as rope-like structures (RLS). These are analogous to a macroscopic fishnet, which resists extension, but crumples or compresses easily. Such a RLS then supports tensile loads but no compressive loads. This means that only attractive/contractile forces can result from interactions mediated through such a structure.

To illustrate how net contractility can arise from motors interacting with a RLS, we consider the following simple problem. Being random networks, RLS are apolar: at any given point in space, they are likely to have actin filaments of random orientation. Thus, when a motor binds to the RLS, its motion can be regarded as a random walk with a step length that is expected to be small if the motors are nonprocessive. We first consider two random walkers (RWs) that are rigidly coupled together; e.g., in a large myosin aggregate (see Fig. S5*A*, *Upper*), as we find in stage 2 of myosin driven actin reorganization (see Fig. 4 of main text). These are allowed to interact with an idealized RLS (Fig. S5*A*, *Lower*) that is assumed to be inextensible, but to buckle under the slightest compressive load.

The probability distribution for the contour length s between the RWs—kept a fixed distance $x = l$ apart—satisfies

$$\frac{\partial P(s,t)}{\partial t} = D\frac{\partial^2 P(s,t)}{\partial s^2}, \quad s > l,$$
$$P(s,0) = 2\delta(s-l), \quad \frac{\partial P(l,t)}{\partial s} = 0.$$

The diffusion constant $D = \Delta s^2/(2\Delta t)$ is set by the step size Δs and stepping time Δt for the RWs. The resulting spreading half Gaussian

$$P(s,t) = \frac{e^{-(s-l)^2/(4Dt)}}{\sqrt{\pi D t}}, \quad s > l,$$

gives the average amount of the rope pulled in between the RWs as a function of time

$$\langle s(t)\rangle - l = \sqrt{4Dt/\pi}.$$

The contraction is diffusive, and acts best over short distances. This idealized case where an asymmetric load response leads to contraction over time could be generalized to more realistic situations describing, for example, myosin filaments in a focus interacting with a disordered actin network structure (see Fig. S5*A*, *Upper*). With a bias, which could be thought of as capturing the network turnover bridging parts of buckled structures, the rate of contraction would remain finite also over large distances. The unbiased model of Fig. S5*A* is numerically realized 10 times in Fig. S6*B*, starting with $s = l = 100\Delta s$.

We next consider the case of RWs that are not connected, but interact dissipatively through the background (see Fig. S5*C*)—mimicking, for example, two myosin foci both interacting with the same buckle prone actin structure and a dissipative background network (corresponding to stage 3 in Fig. 4 of the main text). Simultaneous pulling on a taut structure will bring the walkers together whereas simultaneous compression will make the RLS buckle and arc-length will be gathered in between the RWs while they remain fixed in space. This asymmetry drives the RWs together over time. According to the above, the contour length between the RWs performs a random walk, while the distance between RWs tracks the minimum distance attained by this random walk up to the present time (see Fig. S5*D*). The probability over the contour distance s again satisfies the diffusion equation

$$\frac{\partial P(s,t)}{\partial t} = D\frac{\partial^2 P(s,t)}{\partial s^2}.$$

The transition-time distribution $\Psi(\tau,\Delta x)$ for taking the step in real space $x \to x + \Delta x$, starting with a taut rope $x = s$, can be calculated as

$$\Psi(\tau,\Delta x) = \frac{\Delta x e^{-\Delta x^2/(4Dt)}}{4\sqrt{\pi D}\tau^{3/2}}.$$

The distribution of transition times is broad, with a wide-tail falling off as $1/\tau^{3/2}$. The average time to take a step forward diverges in this model, indicating that the dynamics is highly irregular with long pauses to contraction. The average velocity remains positive

$$\langle v\rangle = \langle \Delta x/\tau\rangle = \int_0^\infty d\tau(\Delta x/\tau)\Psi(\tau,\Delta x) = D/\Delta x,$$

showing the possibility of rapid contraction over short distances. This simple model can be extended to the situation with multiple RLS connecting the RWs. Here, the distance between RWs would track the minimum contour length attained in any one of the multiple diffusion processes. In Fig. S5*E* we show an example of an experimentally measured time evolution of the distance between the two contracting myosin foci shown in Movie S13. The motion is clearly directional, but seems interspersed by pauses of apparent inactivity—as is the case for the simple model presented here.

These simple examples show idealized cases where an asymmetric load response of the material connecting the motors results in an overall net contraction. We could further consider more complex material responses, allowing for reversible and irreversible deformations of the background network and the RLS. The limits we have considered assume the existence of floppy portions of the network with slack that can be "pulled-out." Whereas this is expected to be the case for realistic networks, it is not captured by the largely continuum mechanical models that have been used to date to model these networks, usually on larger scales. To the extent that continuum linear elasticity applies, the mechanism we propose would not result in contractility. Continuum mechanics, however, is unlikely to describe well the relatively loose meshwork of filaments expected for our system at the microscopic scale of a few microns.

1. Pardee J, Spudich J (1982) Purification of muscle actin. *Methods Enzymol* 85:164–181.
2. Margossian S, Lowey S (1982) Preparation of myosin and its subfragments from rabbit skeletal muscle. *Methods Enzymol* 85:55–71.
3. DeBiasio R, Wang L, Fisher G, Taylor D (1988) The dynamic distribution of fluorescent analogues of actin and myosin in protrusions at the leading edge of migrating Swiss 3T3 fibroblasts. *J Cell Biol* 107:2631–45.
4. Kolega J (1998) Fluorescent analogues of myosin II for tracking the behavior of different myosin isoforms in living cells. *J Cell Biochem* 68:389–401.
5. Mizuno D, Tardin C, Schmidt CF, MacKintosh FC (2007) Nonequilibrium mechanics of active cytoskeletal networks. *Science* 315:370–373.
6. Koretz J (1982) Hybridization and reconstitution of thick-filament structure. *Methods Enzymol* 85(Pt B):20–55.
7. Huxley H (1963) Electron microscope studies on the structure of natural and synthetic protein filaments from striated muscle. *J Mol Biol* 7:281–308.

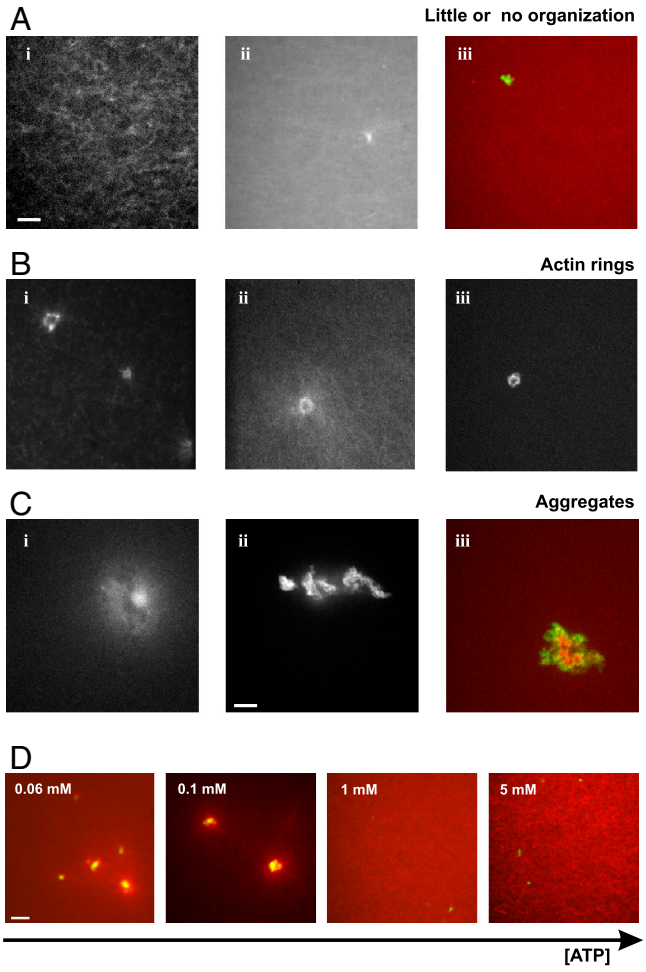

Fig. S1. Myosin processivity affects in vitro actin active organization. (*A–C*) Minifilaments of skeletal myosin II assembled at 150 mM KCl are seldom able to reorganize actin networks. (*A*) Fluorescent micrographs of active networks with labeled actin (*i*, *ii*) and doubly labeled with actin in red and myosin in green (*iii*). In the presence of myosin II minifilaments, networks often remain overall homogenous without evidence of active foci formation. (*B*) Fluorescent micrographs of active networks with labeled actin. Rings rarely emerge in actin networks in the presence of minifilaments. (*C*) Fluorescent micrographs of active networks with labeled actin (*i*, *ii*) and doubly labeled with actin in red and myosin in green (*iii*). Often, disordered aggregates appear in the network. Scale bar, 5 μm. All fields of view are the same size except (*C ii*) where the scale bar is 10 μm. (*D*) ATP concentration modulates pattern formation in active actin-myosin networks. Fluorescence micrographs of actomyosin networks (actin in red and myosin in green) taken at different ATP concentrations. At levels of 60–100 μM ATP, myosin is sufficiently processive to cause the formation of actomyosin condensates. In contrast, the actin network remains homogeneous and the myosin filaments remain homogeneously dispersed in the network at mM ATP concentrations, indicating that myosin is not sufficiently processive to cause network reorganization. Scale bar, 5 μm. Samples from panels *A–D* contain 1:200 myosin:actin and the crosslinker:actin ratio is 1:1,000.

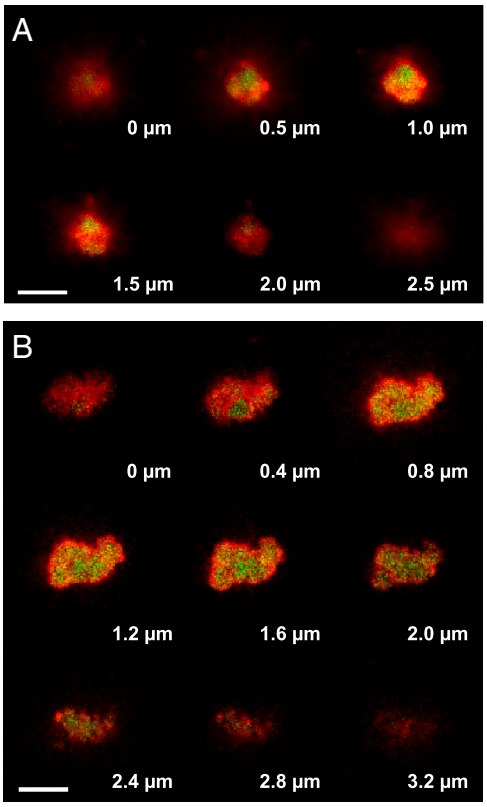

Fig. S2. Stack of confocal microscopy x-y slices of fluorescently labeled actin-myosin condensates (myosin in green and actin in red). Scale bars, 5 μm. (*A*) Sequence of xy-slices of an actomyosin condensate at 1:200 motor:actin ratio. Myosin is in the center, and an actin shell surrounds it. (*B*) Sequence of xy-slices of a superaggregate composed of several actomyosin condensates at 1:50 motor:actin ratio. Each myosin focus within the condensate is surrounded by a shell of actin.

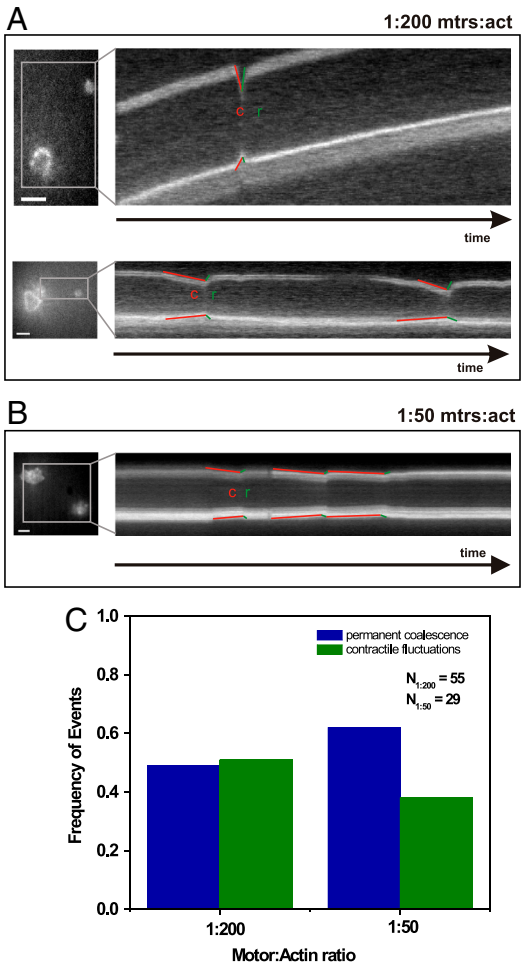

Fig. S3. Myosin concentration influences the dynamics of actin network contractility. (*A* and *B*) Snapshots of actomyosin condensates (labeled actin only) with corresponding kymographs of contractile fluctuation events. Red lines indicate contracting period (*c*) and green lines indicate relaxation/recoil (*r*). Scale bars, 5 μm. (*A*) (*Upper*) Two ring-like actin structures move toward each other and relax. Total kymograph duration 612 s. (*Lower*) Two small actin structures move toward each other and relax two consecutive times. Total kymograph duration 133 s. The crosslinker:actin ratio is 1:1,000 and the myosin:actin ratio is 1:200. (*B*) Two large actin structures slowly move toward each other and then relax three consecutive times. Total kymograph duration 154 s. The crosslinker:actin ratio is 1:1,000 and the myosin:actin ratio is 1:50. (*C*) Statistics of permanent coalescence versus contractile fluctuation events of actomyosin condensates in actin-myosin networks as a function of myosin:actin molar ratio.

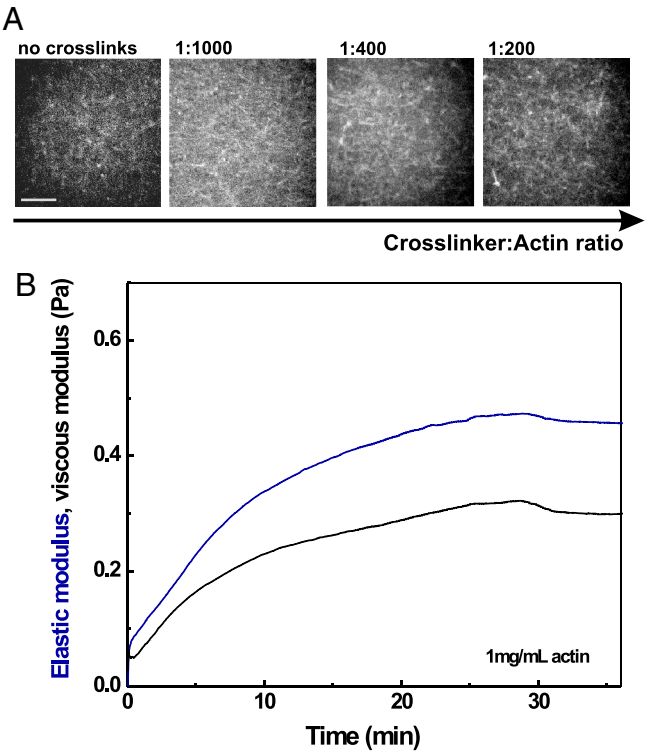

Fig. S4. Passive actin network formation. (*A*) Fluorescence micrographs of passive actin networks (no myosin) with different cross-linker (biotin-actin) densities. Cross-linking does not change the overall network structure up to a concentration of 0.12 μM (at an actin concentration of 23.8 μM). Above this threshold, the network structure looks somewhat coarser, but no distinct aligned or ordered patterns are visible. Actin was polymerized in the presence of 50 mM KCl, 2 mM $MgCl_2$ and 100 μM MgATP. Scale bar, 10 μm. (*B*) Polymerization curve of a passive actin network (no myosin) at 1 mg/mL at 25 °C, obtained by measuring the elastic and viscous shear moduli in a stress-controlled rheometer (Anton Paar MCR501), using oscillatory shear with a small strain amplitude of 0.5%. The curves are averages of four independent experiments using stainless steel CP20-1 and PP20 geometries.

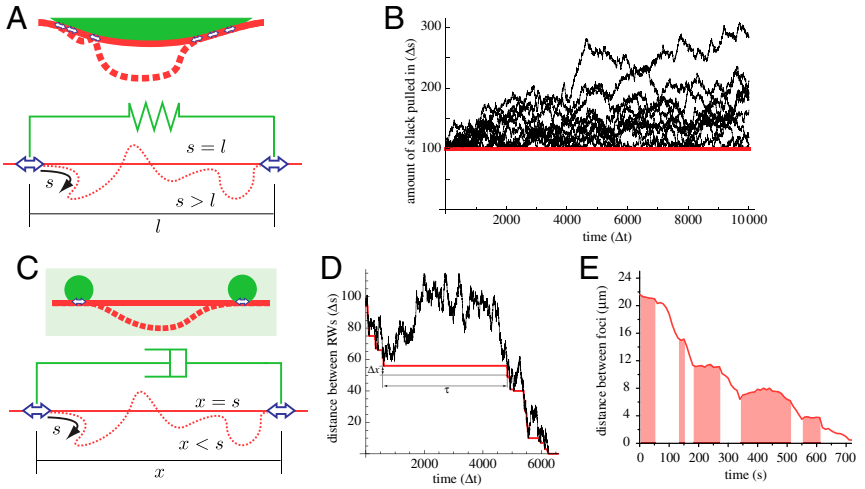

Fig. S5. (*A*) The random rope-like structures (RLS) can either be taut (solid red) or buckled (dotted red) between the random walkers (blue arrows). On top we illustrate a RLS interacting with a larger aggregation of random walkers (RWs) such as present in myosin foci. Below is the idealized model with only two rigidly coupled (green) RWs. Though the walkers are able to push in slack between themselves they are unable to extend a taut RLS. (*B*) The amount of RLS contour length between the walkers, *s*, performs a random walk reflected at $s = l$ (RLS is taut). Here we show time traces for 10 different realizations, all starting at $s = l = 100\Delta s$. (*C*) The RLS can either be taut (solid red) or buckled (dotted red) between the random walkers (blue arrows). On top we illustrate two myosin foci immersed in a viscous background and interacting with a buckle prone network structure. Below we show the simplified model describing this situation. The walkers are unaffected by the viscosity coupling them together through the background network (green dash-pot). When the RW both stochastically pull on an already taut RLS it brings the RWs together. Though the viscous coupling is assumed weak enough not to hinder the motors, it is assumed to be strong enough to induce buckling as soon as the rope is put under compression by the motors. If the RWs randomly compress the RLS, it buckles as material is fed in between the RWs. This excess material has to be pulled-out before the RLS can be made taut and move the RWs closer in space. (*D*) In black we show a numerical realization of the diffusion of the contour length, and in red the corresponding distance between the RWs. (*E*) Experimentally measured distance between the two contracting myosin foci shown in Movie S13. Shaded areas indicate regions where the connecting structure may be under compression, rendering the foci immobile.

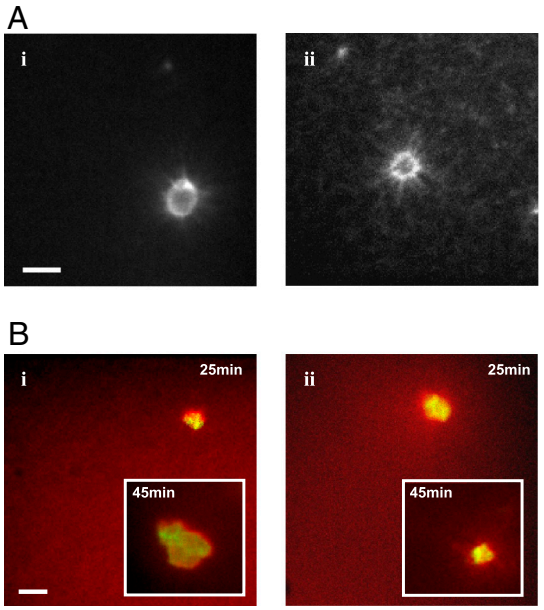

Fig. S6. Active pattern formation in actomyosin networks is not affected by actin dynamics. (*A*) Stabilizing actin filaments does not alter the multistage coarsening process. (*i*) Fluorescent micrograph of a network of labeled actin and unlabeled myosin filaments (myosin : actin ratio is 1 : 200) 35 min after polymerization in the presence of phalloidin (phalloidin : actin molar ratio is 1 : 1). Image shows example of a ring-like actin structure with a size of about 5 μm. The cross – linker : actin ratio is 1 : 1,000. Scale bar, 5 μm. (*ii*) Fluorescent micrograph of control network without phalloidin. (*B*) Mixing preformed actin filaments with myosin filaments does not alter the multistage coarsening process. (*i*) Fluorescent micrograph of a network of labeled actin filaments and myosin filaments (myosin : actin ratio is 1 : 200) 25 min after mixing. Image shows example of an actin/myosin condensate with a size of approximately 4 μm. Scale bar, 5 μm. (*Inset*) Example of a condensate 45 min after mixing. The cross – linker : actin ratio is 1 : 1,000. (*ii*) Fluorescent micrograph of control network 25 min after mixing of preformed myosin filaments with monomeric actin. (*Inset*) Example of a condensate 45 min after mixing.

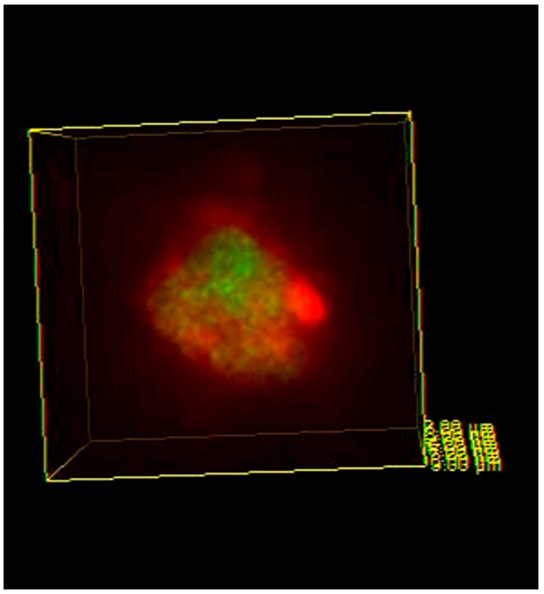

Movie S1. Reconstruction of a 3D stack of 40 fluorescence images of an actin/myosin condensate formed in stage 2 of the multistage coarsening process, obtained using confocal microscopy. Actin (shown in red) accumulates in a dense, disordered shell all around the surface of a globular myosin aggregate (shown in green). The cross – linker : actin ratio is 1 : 1,000 and the myosin : actin ratio is 1 : 200. Corresponding 2D slices are shown in Fig. S2*A*.
Movie S1 (AVI)

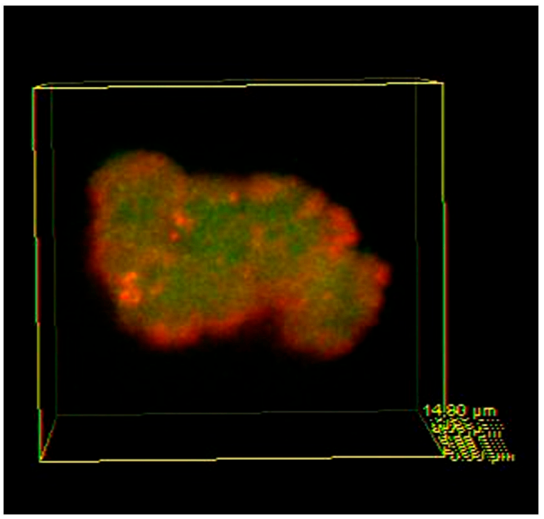

Movie S2. Reconstruction of a three-dimensional stack of 50 fluorescence images of a superaggregate of multiple actin (red)/myosin (green) condensates formed in stage 3 of the multistage coarsening process, obtained using confocal microscopy. The cross – linker : actin ratio is 1 : 1,000 and the myosin : actin ratio is 1 : 50. Corresponding 2D slices are shown in Fig. S2*B*.

Movie S2 (AVI)

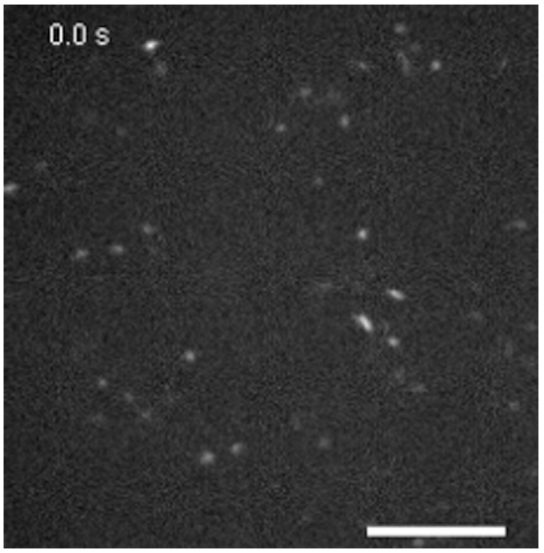

Movie S3. Fluorescently labeled myosin filaments are initially homogeneously distributed throughout the actin network (actin not labeled). In the first 5 min after sample preparation (stage 1 of the multistage coarsening process), they move in an apparently diffusive fashion either through the mesh or actively in a preferred direction, presumably walking along actin filaments. Myosin filaments that meet sometimes fuse into small aggregates. No cross-linkers were added and the myosin : actin ratio is 1 : 300. White arrows represent examples of active walks. Movie total duration is 110 s, 10× real frame rate. Scale bar is 10 μm.

Movie S3 (AVI)

Movie S4. Cropped region of Movie S3, where two fluorescently labeled myosin filaments (or small aggregates thereof) fuse upon meeting. Movie total duration is 55 s, 5× real frame rate. Scale bar is 5 μm.

Movie S4 (AVI)

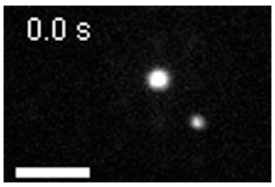

Movie S5. At the beginning of stage 2 of the multistage coarsening process, two myosin foci in an unlabeled actin network abruptly and permanently coalesce with each other as a result of network contractility. The larger one is virtually immobile whereas the small one suddenly approaches and merges with it. The cross – linker : actin ratio is 1 : 1,000 and the myosin : actin ratio is 1 : 200. Movie total duration is 45 s, 5× real frame rate. Scale bar is 5 μm.
Movie S5 (AVI)

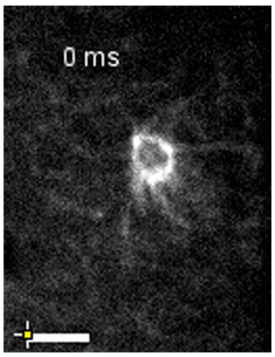

Movie S6. During stage 2 of the multistage coarsening process, a ring-like actin pattern incorporates a fragment of the surrounding actin network (indicated by the white arrow; note that myosin is not labeled). The cross – linker : actin ratio is 1 : 1,000 and the myosin : actin ratio is 1 : 200. Movie total duration is 12 s, 3× real frame rate. Scale bar is 5 μm.
Movie S6 (AVI)

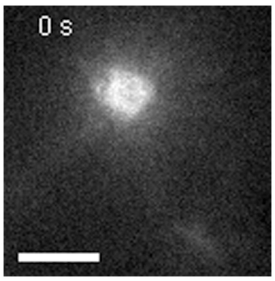

Movie S7. An actin condensate incorporates multiple fragments of the surrounding actin network (myosin is not labeled). The cross – linker : actin ratio is 1 : 1,000 and the myosin : actin ratio is 1 : 200. White arrows represent examples of network fragments being dragged in by the actin ring-like pattern. Movie total duration is 12.3 min, 50× real frame rate. Scale bar is 10 μm.
Movie S7 (AVI)

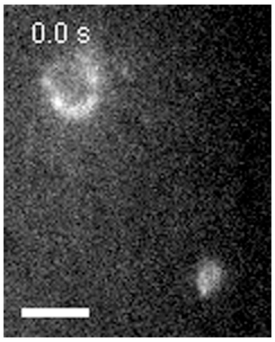

Movie S8. Example of a contractile fluctuation event, where two actin ring-like structures move toward each other and suddenly relax (myosin is not labeled). The parallel white arrows indicate the movements toward and away from each other. The cross – linker : actin ratio is 1 : 1,000 and the myosin : actin ratio is 1 : 200. Movie total duration is 52 s, 10× real frame rate. Scale bar is 10 μm.

Movie S8 (AVI)

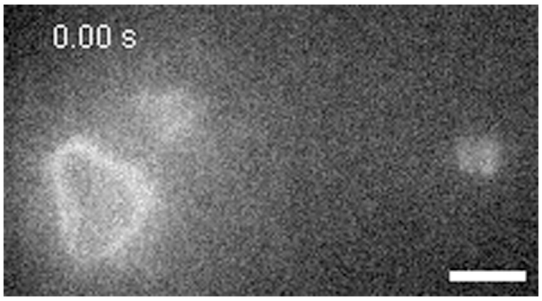

Movie S9. Example of a repeated contractile fluctuation event, where two small actin ring-like structures move toward each other and slowly relax two consecutive times (myosin is not labeled). White circles indicate the beginning of active events. The cross – linker : actin ratio is 1 : 1,000 and the myosin : actin ratio is 1 : 200. Movie total duration is 117 s, 5× real frame rate. Scale bar is 5 μm.

Movie S9 (AVI)

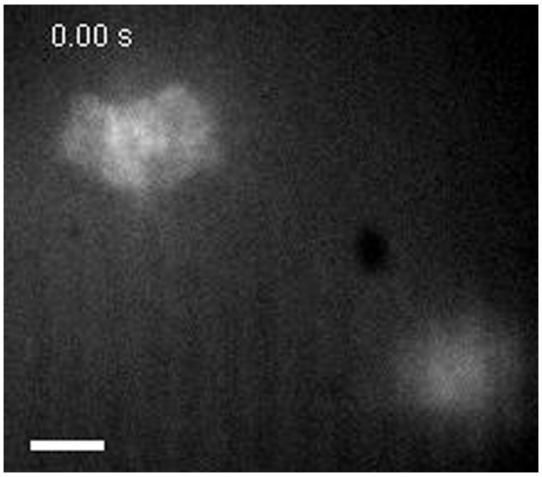

Movie S10. Example of a repeated contractile fluctuation event, where two large actin structures move toward each other and slowly relax three consecutive times (myosin is not labeled). White circles indicate the beginning of active events. No cross-linkers were added. The myosin : actin ratio is 1 : 50. Movie total duration is 104 s, 5× real frame rate. Scale bar is 5 μm.

Movie S10 (AVI)

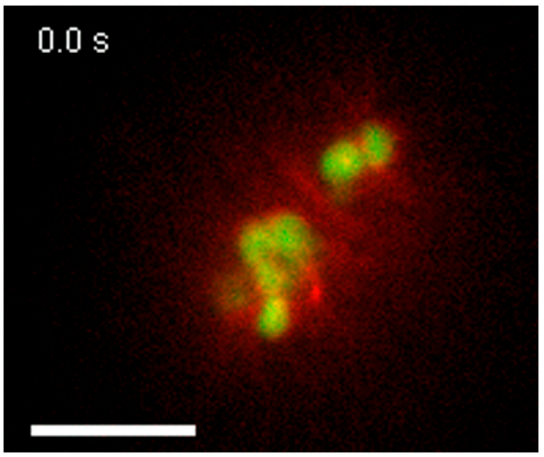

Movie S11. Example of a permanent coalescence event, where two actin (red)/myosin (green) condensates coalesce and crumple the actin network between them. The cross – linker : actin ratio is 1 : 1,000 and the myosin : actin ratio is 1 : 200. The white arrow represents an actin network fragment (in red) that becomes compressed in between the two structures. Movie total duration is 62 s, 10× real frame rate. Scale bar is 10 μm.
Movie S11 (AVI)

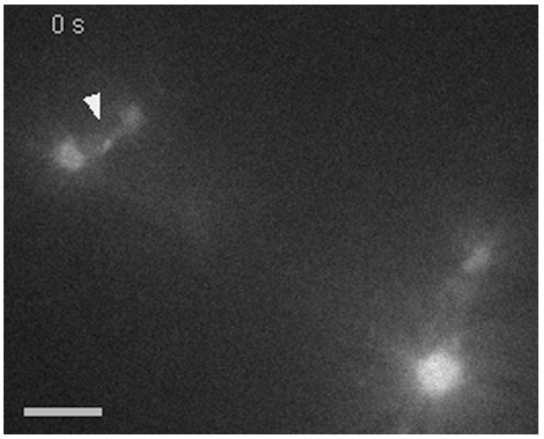

Movie S12. Actin cables form in an actin/myosin network due to contractility. Several actin/myosin condensates appear to be momentarily connected by bundle-like actin structures that collapse when foci approach each other or after foci walk along and drag them. The cross – linker : actin ratio is 1 : 1,000 and the myosin : actin ratio is 1 : 200. White arrows represent examples of such cables emerging. Movie total duration is 22.7 min, 100× real frame rate. Scale bar is 10 μm.
Movie S12 (AVI)

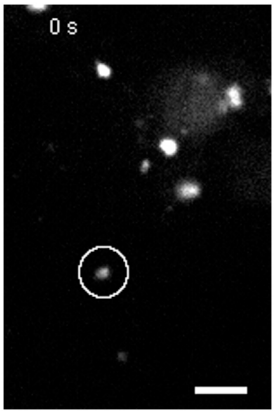

Movie S13. Example of a myosin focus coalescing in an intermittent fashion with a cluster of foci. The cross – linker : actin ratio is 1 : 1,000 and the myosin : actin ratio is 1 : 200. The white circle indicates the focus moving toward the cluster in formation. Movie total duration is 16.5 min, 100× real frame rate. Scale bar is 5 μm.

Movie S13 (AVI)

Table S1. Different class II myosins have distinct kinetic behaviors

Organism	V_{max} (s^{-1})	K_{ATPase} (μM)	Sliding velocity (μm/s)	Duty ratio (%)
		Skeletal muscle myosin II		
Rabbit	86.1 (1)	14 (1)	2.5* (2)	Approximately 4 (3)
Chicken			4.6† (2)	
		Nonmuscle myosin IIA		
Human	0.17 (4)	72 (4)	0.29 (5)	Approximately 5 (4)
		Nonmuscle myosin IIB‡ (6)		
Human	0.13	59	0.05	23
		Nonmuscle myosin II-C‡ (7)		
Mouse	0.16	4.6	0.04	—
		Smooth muscle myosin II		
Chicken	0.7 (8)	59 (8)	0.58 (3)	Approximately 4 (3)

Summary of literature values for the kinetic parameters of actin-activated MgATPase activity of various types of myosin II. Buffer conditions in which variables were measured are indicated together with the literature reference.

ATPase assay: 4 mM Imidazole, 4 mM $MgCl_2$, 10 mM KCl, 1 mM DTT, 1 mM NaN_3, 3 mM NaATP, pH 7.0, 37 °C (1). In vitro motility: 25 mM Imidazole, 1 mM EGTA, 4 mM $MgCl_2$, 1 mM DTT, 25 mM KCl, 1 mM ATP, pH 7.4, 30 °C (2). In vitro motility: 25 mM Imidazole, 1 mM EGTA, 4 mM $MgCl_2$, 10 mM DTT, 1 mMATP, pH 7.4 30 °C (3). ATPase assay: 10 mM 3-(N-morpholino)propanesulfonic acid (MOPS), 0.15 mM EGTA, 2 mM $MgCl_2$, pH 7.0, 25 °C (4). In vitro motility: 20 mM MOPS, 0.1 mM EGTA, 5 mM $MgCl_2$, 80 mM KCl, 1 mM ATP, pH 7.4, 30 °C (5). ATPase assay: 10 mM MOPS, 0.15 mM EGTA, 2 mM $MgCl_2$, 1 mM ATP, pH 7.0, 25 °C (6). ATPase assay: 20 mM MOPS, 0.1 mM EGTA, 2 mM $MgCl_2$, 0.2 mM $CaCl_2$, 1 mM ATP, pH 7.0, 25 °C . In vitro motility: 20 mM MOPS, 50 mM KCl, 0.1 mM EGTA, 5 mM $MgCl_2$, 1 mM ATP, 50 mM DTT, pH 7.4, 30 °C (7). ATPase assay: 5 mM Tris, 1 mM EGTA, 1 mM $MgCl_2$, 10 mM KCl, 0.2 mM $CaCl_2$, 1 mM ATP, pH 7.0, 25 °C (8).

*ATP (0.1 mM).

†ATP (1 mM).

‡Nonspliced isoforms NMII-B0 and C0.

1 Reniscow D, Deacon JC, Warrick HM, Spudich JA, Leinwand LA (2010) Functional diversity among a family of human skeletal muscle myosin motors. *Proc Natl Acad Sci USA* 107:1053–1058.

2 Toyoshima YY, Kron SJ, Spudich JA (1990) The myosin step size: Measurement of the unit displacement per ATP hydrolyzed in an in vitro assay. *Proc Natl Acad Sci USA* 87:7130–7134.

3 Harris DE, Warshaw DM (1993) Smooth and skeletal muscle myosin both exhibit low duty cycles at zero load in vitro. *J Biol Chem* 268:14764–14768.

4 Kovács M, Wang F, Hu A, Zhang Y, Sellers JR (2003) Functional divergence of human cytoplasmic myosin II: kinetic characterization of the nonmuscle IIA isoform. *J Biol Chem* 278:38132–38140.

5 Wang F, Harvey EV, Conti MA, Wei D, Sellers JR (2000) A conserved negatively charged amino acid modulates function in human nonmuscle myosin IIA. *Biochemistry* 39:5555–5560.

6 Wang F, et al. (2003) Kinetic mechanism of nonmuscle myosin IIB: Functional adaptations for tension generation and maintenance. *J Biol Chem* 278:27439–27448.

7 Jana SS, et al. (2009) An alternatively spliced isoform of nonmuscle myosin II-C is not regulated by myosin light chain phosphorylation. *J Biol Chem* 284:11563–11571.

8 Marston SB, Taylor EW (1980) Comparison of the myosin and actomyosin ATPase mechanisms of the four types of vertebrate muscles. *J Mol Biol* 139:573–600.

Table S2. Quantification of the size of actomyosin condensates observed in active networks containing varying concentrations of myosin motors (compare to Fig. 3*B*) and biotin-streptavidin cross-linkers (compare to Fig. 3*C ii*), and quantification of contraction speeds of coalescing condensates (compare to Fig. 3*C i*)

Fig 3B

Motor:actin ratio	⟨Size⟩ (μm)	SD (μm)	N		
1:300	1.75	±0.72	27		
1:200	2.36	±1.14	18		
1:50	5.34	±4.08	39		
ANOVA test	df	SS	MS	F	*P*
Model	2	239	119	14.4	4.3×10^{-6}
Error	81	669	8.3	-	-
Total	83	808	-	-	-

$P \ll 0.001$: populations are significantly different.

Fig 3Ci—speed

Crosslinker:actin ratio	Speed (μm/s)	SD (μm/s)	N
No cross-linkers	0.10	0.05	3
1:1,000	0.63	0.20	4
1:400	0.51	0.11	2
1:200	0.03	0.02	4

Fig 3C ii—size

Crosslinker:actin ratio	⟨Size⟩ (μm)	SD (μm)	N		
No cross-linkers	2.30	0.91	20		
1:1,000	1.40	0.89	69		
1:400	0.98	0.28	16		
1:200	1.96	0.92	25		
ANOVA test	Degrees of freedom (df)	Sum of squares (SS)	Mean square (MS)	F	*P*
Model	3	22	7.4	10.2	4.4×10^{-6}
Error	126	91	0.7	—	—
Total	129	113	—	—	—

$P \ll 0.001$: Populations are significantly different.

Statistical analyses were performed using the ANOVA test in Origin Pro8.

Table S3. In vivo assembled myosin II foci and foci formed in vitro have a similar size

Organism	Size (μm)	Reported size	Estimated size	Velocity (μm/s)	Reference
		Contractile ring formation			
Saccharomyces pombe	≤0.5–1	no	from Fig. 3*D*	0.03	1
Wound healing					
Xenopus oocyte	1–4	no	from Fig. 7*C*	0.2–5.8	2
		Developing embryos			
Drosophila	≤5	no	from Fig. 3*I*	none reported	3
Drosophila	approximately 1	no	from Fig. 1*A*, *Inset*	none reported	4
Drosophila	0.5–2	no	from Fig. 2*C*	0.043 ± 0.016	5
Cortical flows					
C.elegans	2.21 ± 1.16	yes: Fig. S6*C*	no	0.24 ± 0.04	6

Summary of reported or estimated sizes of myosin II foci in different organisms and in different cellular or developmental stages.

1 Vavylonis D, Wu J, Hao S, O'Shaughnessy B, Pollard T (2008) Assembly mechanism of the contractile ring for cytokinesis by fission yeast. *Science* 319:97–100.
2 Mandato C, Bement W (2001) Contraction and polymerization cooperate to assemble and close actomyosin rings around Xenopus oocyte wounds. *J Cell Biol* 154:785–797.
3 Blanchard GB, Murugesu S, Adams RJ, Martinez-Arias A, Gorfinkiel N (2010) Cytoskeletal dynamics and supracellular organisation of cell shape fluctuations during dorsal closure. *Development* 137:2743–2752.
4 Franke J, Montague R, Kiehart D (2005) Nonmuscle myosin II generates forces that transmit tension and drive contraction in multiple tissues during dorsal closure. *Curr Biol* 15:2208–2221.
5 Martin A, Kaschube M, Wieschaus E (2009) Pulsed contractions of an actin-myosin network drive apical constriction. *Nature* 457:495–499.
6 Mayer M, Depken M, Bois JS, Julicher F, Grill SW (2010) Anisotropies in cortical tension reveal the physical basis of polarizing cortical flows. *Nature* 467:617–621.